ACS APPLIED MATERIALS & INTERFACES

Research Article

www.acsami.org

Infiltration of Polymer Hole-Conductor into Mesoporous Titania Structures for Solid-State Dye-Sensitized Solar Cells

Monika Rawolle,[†] Kuhu Sarkar,[†] Martin A. Niedermeier,[†] Markus Schindler,[†] Philipp Lellig,[‡] Jochen S. Gutmann,[‡,§] Jean-François Moulin,[∥] Martin Haese-Seiller,[∥] Angela S. Wochnik,[⊥] Christina Scheu,[⊥] and Peter Müller-Buschbaum*[,†]

[†]Lehrstuhl für Funktionelle Materialien, Physik-Department, Technische Universität München, James-Franck-Strasse 1, 85748 Garching, Germany

[‡]Max Planck Institute for Polymer Research, Ackermannweg 10, 55128 Mainz, Germany

[∥]Helmholtz Zentrum Geesthacht, Institut für Werkstoffforschung, Abteilung WPN, Instrument REFSANS, FRM II, Lichtenbergstrasse 1, 85748 Garching, Germany

[⊥]Department of Chemistry, Ludwig-Maximilians-University Munich, Butenandtstrasse 11, 81377 München, Germany

ABSTRACT: The degree of filling of titania nanostructures with a solid hole-conducting material is important for the performance of solid-state dye-sensitized solar cells (ssDSSCs). Different ways to infiltrate the hole-conducting polymer poly(3-hexylthiophene) (P3HT) into titania structures, both granular structures as they are already applied commercially and tailored sponge nanostructures, are investigated. The solar cell performance is compared to the morphology determined with scanning electron microscopy (SEM) and time-of-flight grazing incidence small-angle neutron scattering (TOF-GISANS). The granular titania structure, commonly used for ssDSSCs, shows a large distribution of particle and pore sizes, with porosities in the range from 41 to 67%, including even dense parts without pores. In contrast, the tailored sponge nanostructure has well-defined pore sizes of 25 nm with an all-over porosity of 54%. Filling of the titania structures with P3HT by solution casting results in a mesoscopic P3HT overlayer and consequently a bad solar cell performance, even though a filling ratio of 67% is observed. For the infiltration by repeated spin coating, only 57% pore filling is achieved, whereas filling by soaking in the solvent with subsequent spin coating yields filling as high as 84% in the case of the tailored titania sponge structures. The granular titania structure is filled less completely than the well-defined porous structures. The solar cell performance is increased with an increasing filling ratio for these two ways of infiltration. Therefore, filling by soaking in the solvent with subsequent spin coating is proposed.

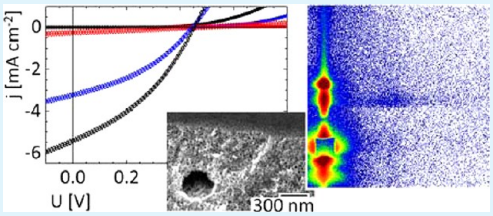

KEYWORDS: *titania, mesoporous nanostructure, filling ratio, P3HT, solid-state dye-sensitized solar cells, GISANS*

INTRODUCTION

As an alternative to tackle today's energy challenges, dye-sensitized solar cells (DSSCs) have already been under discussion to supplement current energy conversion technologies since the 1990s.[1,2] In the case of classical DSSCs, also called Grätzel cells, high efficiencies of more than 12% are reached with a liquid iodine-based electrolyte as a hole-conducting material and titania as an electron conductor.[3] Because of the high efficiencies, DSSCs are foreseen to contribute significantly to the power generation by the year 2020.[4] However, so far, commercialization was not successful, as the corrosive liquid electrolyte faces problems of chemical stability and a need for tight sealing. The problems related to sealing can be overcome by replacing the liquid electrolyte with a solid-state hole-conductor in the case of so-called solid-state dye-sensitized solar cells (ssDSSCs).[5] For this type of solar cell, efficiencies have reached around 7% today, in cases where small-molecule hole-conductors are used. If a polymer hole-conductor like poly(3-hexylthiophene) (P3HT) is utilized, efficiencies are lower with values up to 5%.[3] One important aspect for ssDSSCs is the infiltration of small-molecule or polymer hole-conductors into existing electron-conductor morphologies, such as titania nanostructures. In the case of small molecules, Schmidt-Mende and Grätzel have shown qualitatively how strongly the solar cell performance depends on the pore-filling ratio.[6] By different ways of infiltration, the filling ratio was improved as measured quantitatively at local spots of the samples.[7] However, a further improvement of filling ratios is still necessary.[8] It is suggested that the filling is among the most important aspect in the search for alternate hole-conducting materials.[9] For example, the infiltration of titania nanostructures with P3HT was investigated locally by depth profiling. Very low infiltration ratios or limitations of filling to the pore walls,[10,11] which resulted in bad packing of the polymers, both gave rise to a low conductivity of the hole-conductor. Already in 2003, Coakley and McGehee et al.

Received: October 8, 2012
Accepted: December 30, 2012
Published: December 31, 2012

investigated the infiltration of mesoporous titania with P3HT[11] and reported degrees of filling of 33% only as probed at local spots of the films by using X-ray photoemission spectroscopy (XPS) depth profiling. The low conductivity of the infiltrated polymer is responsible for the low efficiencies of photovoltaic cells made from the combination of mesoporous titania with infiltrated polymer.[12] Infiltration into more regular and straight pores was shown to lead to more ordered polymer structures and consequently to a higher conductivity.[13] In addition, a further step into the direction of optimized solar cells lies in the application of additives to improve crystallinity and consequently conductivity in P3HT, which so far was shown successfully for all-organic solar cells.[14]

In general, nanostructures of titania are very interesting due to their application potential.[15] Most commonly, the titania structures used in photovoltaic applications are prepared from a nanoparticle paste, where the resulting nanostructure consists of granules with a broad size distribution.[16] Enhanced solar cell performance was achieved in the case of electrolyte-based DSSCs by structuring the titania film via the self-assembly of a templating material.[17] Anodization was also used successfully to prepare titania nanotubes for powders with additional light scattering that enhances DSSC performance.[18] The importance of nanostructures for the DSSC performance was also shown for other types of electron conductors, for example, for Nb_2O or ZnO instead of titania[19,20] and for ZnO-titania composites.[21] The combination of metal oxides and conducting polymers has further interesting application potentials, for example, hybrid organic−inorganic light-emitting diodes (HyLEDs),[22] which have to tackle the same challenges.

Titania nanostructures can be obtained by a variety of chemical, physiochemical, or physical techniques,[23] for example, from chemical vapor deposition,[24] electrospinning,[25] growth driven by catalysis,[26] sputtering of titanium with subsequent anodization,[27−29] growth on sacrificial polymer colloids,[30] alignment of nanoparticle building blocks to form colloidal mesocrystals,[31] or sol−gel chemistry.[32−37] One possibility to template nanostructures is the application of amphiphilic block copolymers as a structure-directing agent in combination with sol−gel chemistry.[32,33] This powerful technique gives access to a variety of different morphologies and can also be extended to low preparation temperatures.[34,35] Furthermore, this approach allows one to integrate additional functionality in the titania synthesis step already, and therefore, functional composite materials can be produced in one step.[36,37] A large variety of titania structures are obtained by the combination of sol−gel chemistry and block copolymer templates, from lamellae and nanoparticles via nanorods, nanowires, and nanotubes to nanovesicles and spongelike nanoscale networks.[38−40] Moreover, hierarchical structuring is possible in this approach.[41,42] Further orientation of the structures can be introduced by a surface treatment below a critical film thickness or by the sandwiching between two neutral surfaces during drying.[43] Because of the limited exciton diffusion length in conducting polymers, a spongelike structure with pores of sizes around 30 nm are expected to be especially interesting for ssDSSCs.[44]

So far, investigations concerning the degree of filling of titania with a hole-conducting material have been performed typically with local probes such as XPS depth profiling.[6,7,10−13] To probe nanostructures in thin film geometry in large sample volumes on the order of the pixel size commonly used in ssDSSCs, scattering techniques have been applied successfully.[36,45,46] Grazing incidence small-angle X-ray scattering (GISAXS) allows us to probe such nanostructures statically and also kinetically during growth processes.[47−49] In the case of using neutrons instead of X-rays, the technique is called grazing incidence small-angle neutron scattering (GISANS). A different contrast as compared to GISAXS can be achieved in GISANS, rendering GISANS a very powerful tool.[50,51] Moreover, via deuteration, the scattering contrast could be further enhanced in the case of GISANS, which however was not necessary in the present investigation. In the time-of-flight (TOF) mode, a continuous wavelength spectrum of the neutron beam is used. Historically, the TOF mode has first been applied successfully in neutron reflectometry[52−55] and off-specular scattering.[56−59] Combining the TOF mode with GISANS is a rather recent experimental development with the first successful reports in 2009.[60,61] With this so-called TOF-GISANS, among other information, quantitative values for the porosity of titania nanostructures and the degree of filling of the titania nanostructures with solid hole-conductors can be probed.[62] Furthermore, a depth sensitivity is achieved due to changes in the scattering depth as a function of the neutron wavelength at a fixed incident angle.[63,64] In general, TOF-GISANS allows us to probe the same information with a fixed incident angle and a varied wavelength as GISANS with a monochromatic beam, corresponding to a fixed wavelength, in measurements with a varied incident angle. Regarding the availability of TOF instruments, the main difference lies in the neutron source. At a spallation source, a pulsed neutron beam is supplied, and TOF instruments are common. In contrast, at a neutron reactor, a constant neutron flux can be used for either monochromatization or pulsing with a chopper system, rendering both monochromatic and TOF experiments possible. Recently, TOF-GISANS was used in our group to investigate the filling of a titania sponge structure with the conducting polymer poly(*N*-vinylcarbazole) (PVK) by one time spin coating and by solution casting.[62]

In the present work, the focus lies on the quantitative investigation of three different ways of infiltration of the polymer hole-conductor P3HT into different titania nanostructures. Granular titania structures, as they are obtained from a commercial paste, are compared with block copolymer template-tailored sponge titania nanostructures. The advantages and disadvantages of different filling techniques are focused on, instead of pushing the solar cell performance with additional optimization steps toward record values. With real space imaging using scanning electron microscopy (SEM), qualitative findings about the infiltration of the hole-conductor in the titania structures are obtained. TOF-GISANS measurements yield information about the nanostructures in the whole volume of the film, quantitative information about the porosity of the titania structures, and the degree of filling of the hole-conductor P3HT in the titania pores. Structural and compositional investigations with X-ray reflectivity (XRR), transmission electron microscopy (TEM), and energy dispersive X-ray spectroscopy (EDX) complement the investigations.

EXPERIMENTAL SECTION

Sample Preparation. Solar cells were prepared on fluorine-doped tin oxide (FTO) coated glass in a procedure similar to the one described in reference 65 but with P3HT as the hole-conductor instead of the small-molecule hole-conductor. Briefly, the FTO was patterned by etching with zinc powder and hydrochloric acid (HCl, 18%) and then cleaned with Alconox, ethanol, acetone, and isopropanol in an ultrasonic bath for 10 min each with subsequent

rinsing with the respective solvent and drying in nitrogen flow. The FTO surface was then treated with an oxygen plasma (10 min, 250 W, 0.4 mbar), followed by spin coating of a compact titania layer from a sol as described in reference 66. The spin coating was performed on a Süss MicroTec Delta 6 RC spin coater (2000 rpm, 60 s). The compact titania layer was sintered at 450 °C for 2 h (heating ramp 6.5 K min^{-1}). The samples were immersed in a $TiCl_4$ bath (40 mM, 45 min, 70 °C) before the application of the granular titania from a commercial paste (Solaronix Ti-Nanoxide T) by blade coating. Directly after application of the titania paste, the samples were put on a hot plate (6 min, 120 °C). After calcination (subsequently 325, 375, and 450 °C, each 15 min, heat ramp 15 K min^{-1}), the samples were again immersed in a $TiCl_4$ bath with a subsequent calcination (400 °C, 30 min, heat ramp 25 K min^{-1}). After they were cooled to 80 °C, the samples were immersed in a dye solution (ruthenium dye N-719 in acetonitrile and tert-butanol) for more than 20 h before the infiltration of the polymer hole conductor (regio-regular P3HT, M_W = 50 kg mol^{-1}, Rieke Metals, radius of gyration about 5 nm) in three different ways as described below. After evaporation of gold contacts, the samples were annealed on a hot plate (nitrogen atmosphere, 10 min, 140 °C).

The films for the scattering investigation were prepared on silicon and glass substrates (size 60 × 70 mm^2) precleaned in an acidic bath for 15 min.[67] The granular titania films on silicon substrates were prepared from a commercial paste by blade coating as described above for the solar cell preparation. The tailored titania sponge structures were prepared on glass substrates by the combination of block copolymer-templated sol−gel chemistry with microfluidics as described in reference 68 in detail. For this purpose, the diblock copolymer poly(dimethyl siloxane-*block*-methyl methacrylate poly(ethylene oxide)) [PDMS-*b*-MA(PEO)] was used as the template after the synthesis described in reference 69. HCl (37%) was added to the PDMS-*b*-MA(PEO) solution in THF and 2-propanol, and the titania precursor titanium tetra isopropoxide (TTIP) was added to a mixture of pure solvents (THF and 2-propanol). Both solutions were mixed in a y-shaped microfluidic channel directly before spin coating onto the glass substrates. Titania was uncovered on top of the sample by an argon plasma treatment before calcination in nitrogen atmosphere. As a result, the PDMS converts to a SiOC type ceramic, and a titania-ceramic composite is obtained similar to the one investigated in reference 65. The films were stored in the dye solution for more than 20 h (like the solar cells) before the infiltration of the hole-conducting polymer P3HT.

Three different ways to infiltrate the hole-conductor were investigated. In the first way, 11 times repeated spin coating of a P3HT solution (in toluene with a concentration of 10 mg mL^{-1}) was applied with a wait time of 40 s for distributing the solution before spin coating (2000 rpm, 60 s). This first way of filling by repeated spin coating promises improvement over the common one-time spin coating, because the porous structure can be filled more and more, in case one time spin coating is insufficient. As a second way to infiltrate the P3HT from toluene solution into the titania structures, the solution was cast on the structures and dried in ambient conditions for about 24 h. The so-called solution casting is expected to yield rather high infiltration ratios.[62] The third way to infiltrate the P3HT solution from toluene into the titania nanostructures investigated in the present work is a soaking of the titania films in the pure solvent toluene for more than 45 min, to remove as much of the air inside the nanostructure pores as possible, before applying the P3HT solution with 40 mg mL^{-1} on top (40 s waiting) and subsequently spin coating off the remaining solution (2000 rpm, 60 s). That the air inside of nanopores is removed by immersing of the porous structure inside the solution was shown already both for uncharged and for charged polymer chains.[70]

Film Characterization. Solar cells were characterized with a Keithley digital sourcemeter to measure I−V curves in the dark and under illumination with AM1.5 standard solar spectrum of 1 sun (100 mW cm^{-2}).

SEM measurements of sample cross-sections of the solar cells were performed at an NVision40 FESEM by Carl Zeiss AG (accelerating voltage, 2.5 kV; working distance, 3.5 mm; tilt angle, 50°) after breaking the samples cooled down to liquid nitrogen temperatures. Secondary electron images were taken with the in-lens detector.

XRR measurements were performed with a copper X-ray tube (Cu Kα, λ = 1.54 Å) at a Bruker D8 reflectometer, using a scintillation counter. The reflectivity profile was fitted by a model based on the Parratt algorithm.[71] The theoretical scattering length density (SLD) for X-rays of titania is 3.17 × 10^{-5} $Å^{-2}$. For SiOC, it is 2.40 × 10^{-5} $Å^{-2}$.

TEM investigations were done using a FEI Titan 80-300 (S)TEM microscope equipped with an EDAX detector for EDX measurements and a Gatan Tridiem image filter. Scanning TEM measurements (STEM) were performed with a high-angle annular dark field detector from Fischione Instruments (Model 3000). Cross-section samples for the TEM and STEM investigations were prepared as described by Strecker at al. in reference 72.

GISANS. TOF-GISANS measurements were performed at the REFSANS instrument of the Helmholtz Zentrum Geesthacht at the neutron research reactor FRM II in Garching, Germany,[73,74] using a wavelength range of 2−12.5 Å. The incident angle under which the neutron beam impinged on the samples was chosen between 0.41° and 0.44° for the low wavelengths and between 0.43° and 0.46° for the longer wavelengths. Effects due to gravity, which are more relevant for larger neutron wavelengths, are corrected in the analysis. Except for the effect of gravity, the incident angle was fixed in each scattering experiment. The data were detected at a sample-to-detector distance of 10.52 m on a two-dimensional (2d) detector at a fixed position.[75] The counting time for each sample was about 24 h to have sufficient statistics. A material-specific, characteristic scattering is detected at an exit angle equal to the critical angle α_c for total external reflection of this material. The material-specific critical angle changes with the wavelength λ of the neutrons with $\alpha_c = \lambda(\rho/\pi)^{1/2}$.[62] ρ is the SLD of the material, which is directly proportional to the material density of the probed material. Thus, the critical angles can be determined from the material-specific characteristic scattering, which occurs at an exit angle equal to the critical angle of the material. The corresponding peak in the GISANS data is called the Yoneda peak.[76,77] The SLD can be obtained from the slope of the linear fit of critical angle versus wavelengths of the neutrons used for scattering in the TOF mode, as shown in reference 62. For a porous structure, the SLD is reduced, and the porosity Φ can be calculated as

$$\Phi = 1 - \rho_m/\rho_{theor}$$

where ρ_m is the measured SLD and ρ_{theor} is the theoretical SLD of the compact material. In the case of a porous material, filled with another material like a hole-conducting polymer, the polymer fraction ξ inside the pores can be calculated with the porosities of the unfilled material Φ via

$$\xi = [\rho_{m,filled} - (1 - \Phi)\rho_{theor,TiO_2}]/\rho_{theor,P3HT}$$

where $\rho_{m,filled}$ describes the measured SLD of the filled titania, ρ_{theor,TiO_2} is the theoretical SLD of the compact titania of 2.40 × 10^{-6} $Å^{-2}$, and $\rho_{theor,P3HT}$ is the theoretical SLD of P3HT of 6.65 × 10^{-7} $Å^{-2}$. The theoretical SLD of SiOC for neutrons is 4.99 × 10^{-6} $Å^{-2}$. The penetration depth of the neutrons in the investigated films and consequently also the scattering depth depends on the wavelength of the neutrons.[78] For a fixed incident angle, neutrons with a short wavelength fully penetrate the investigated films, but neutrons with a longer wavelength are scattered at a finite depth of the order of 50 nm (exact value depends on sample). For the investigations of porosity and degree of filling, only the data of neutrons with short wavelengths are used. Therefore, quantitative information is obtained for the whole film volumes.

RESULTS AND DISCUSSION

Solar Cell Performance. The solar cell performance depends strongly on the way of filling of the titania structures. Figure 1 shows I−V data of ssDSSCs for the different ways of infiltration in the case of the granular titania prepared from the

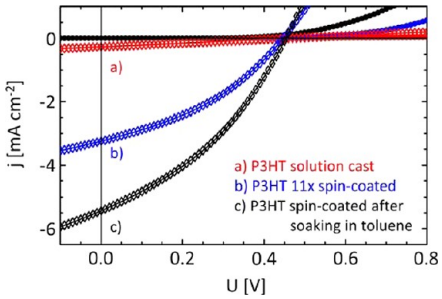

Figure 1. Current–voltage characteristics of ssDSSCs, consisting of granular titania from the commercial paste, filled with P3HT by solution casting (a), 11 times repeated spin coating (b), and spin coating after soaking of the titania film in toluene (c). Dark curves (filled circles) and curves under illumination with simulated sunlight AM1.5 (open diamonds) are shown for each kind of filling.

commercial paste. The most important results are summarized in Table 1. The worst efficiencies η of not more than 0.03% are

Table 1. Overview of Solar Cell Parameters for the Different Kinds of P3HT Infiltration into the Granular Titania Nanostructure

way of filling	U_{OC} (V)	j_{SC} (mA cm^{-2})	FF (%)	η (%)
11 times spin coating	0.45	−3.25	37.0	0.54
solution casting	0.47	−0.27	25.4	0.03
spin coating after soaking in toluene	0.45	−5.44	36.2	0.90

obtained for filling by solution casting. Filling by 11 times repeated spin coating grants already higher efficiencies of up to 0.54% and soaking in toluene with subsequent spin coating of the P3HT solution results in the best efficiencies of up to 0.90%. The efficiencies obtained in the present investigation are clearly not optimized for the highest possible values but rather show the trend of the way of filling for solar cells otherwise prepared in exactly the same way. One possible way to improve the efficiencies lies in the improvement of conductivity in P3HT through additives, as described above.[14] As can be seen from the short-cut current density j_{sc}, lower efficiencies η are mostly due to less extracted charges. In the case of filling by solution casting, a high series resistance is apparent as well from the low slope at the open-circuit voltage and from the much lower filling factor FF. The open-circuit voltage U_{OC} is defined by the choice of materials and is constant for the present measurements.

Real Space Morphology Analysis. The granular titania morphology as probed in real space with cross-sectional SEM is shown in Figure 2a,e. The granules with a size distribution around 15–20 nm are arranged in a loose but irregular manner, and pores with a broad size distribution are visible. Cross-sectional SEM measurements of the granular titania structure filled with P3HT (see Figure 2b–d and f–h) reveal qualitatively poor to rather good infiltration, depending on the way of infiltration, as was observed for small molecules as well.[6] Qualitatively, the filling ratio increases from filling by repeated spin coating via filling by solution casting to filling by soaking in toluene with subsequent spin coating. The lower observed short-cut current densities in the solar cell characteristics (Table 1) can be explained with a lower interfacial area for less complete filling in the case of repeated spin coating. For

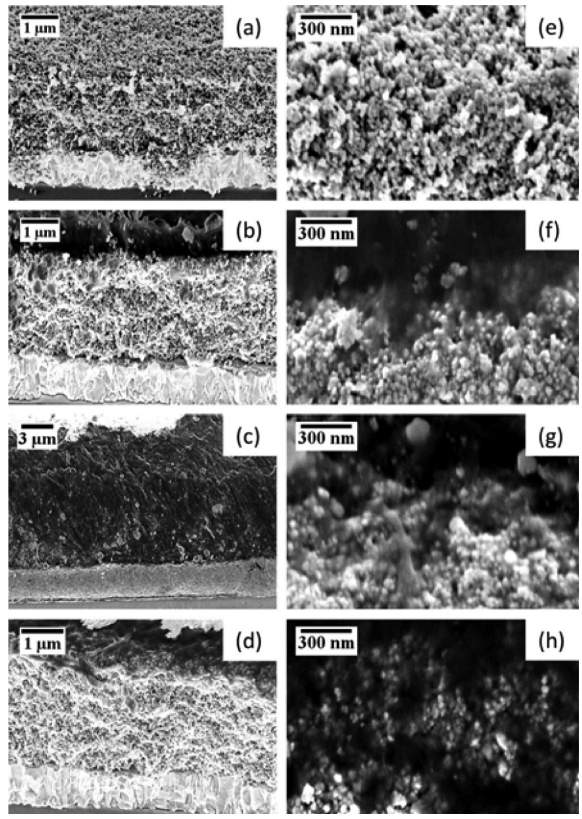

Figure 2. Cross-sectional SEM images of granular titania structure (a, e) and of granular titania filled with P3HT by 11 times repeated spin coating (b, f), by solution casting (c, g), and by soaking in toluene with subsequent spin coating (d, h). In the overview images (a–d), the FTO electrode on the bottom and the gold electrode on top of the P3HT (c, d) are visible.

filling by soaking of the titania film in toluene with subsequent spin coating of the P3HT solution, the filling of the titania pores seems more complete, which agrees with the higher short-cut current density and higher efficiency of the solar cell prepared in otherwise the same way. In the case of the filling by solution casting, the filling seems to be more complete than for repeated spin coating, but the short-cut current density is nevertheless rather low due to the much higher serial resistance. This can be explained by a significantly thicker overlayer of P3HT on top of the titania structure, as can be seen in Figure 2c. This overlayer results in the loss of holes in the thick P3HT layer, leading to the high serial resistance and the low short-cut current density and as a consequence to a very low efficiency. The thick overlayer of P3HT could be removed for example by a plasma etching step or by a further solvent treatment.

For the tailored titania sponge structures, the same trend with respect to filling is observed in the SEM data (see Figure 3). The defined titania sponge structure with hexagonally arranged pores of a diameter of around 25 nm and additional pores of a diameter of around 200 nm is visible in the cross-sectional SEM image in Figure 3a,e. In the bright field TEM image in Figure 4a, the titania sponge structure is shown. The inset displays a detail of the structure at higher magnification, where the porous structure is visible. High-resolution TEM images reveal mesopores with diameters of around 25 nm and in addition crystalline titania domains with diameters of 2–3 nm (Figure 4b). The EDX measurements of the film were done in STEM mode with a spot size of around 1 nm. Twenty EDX

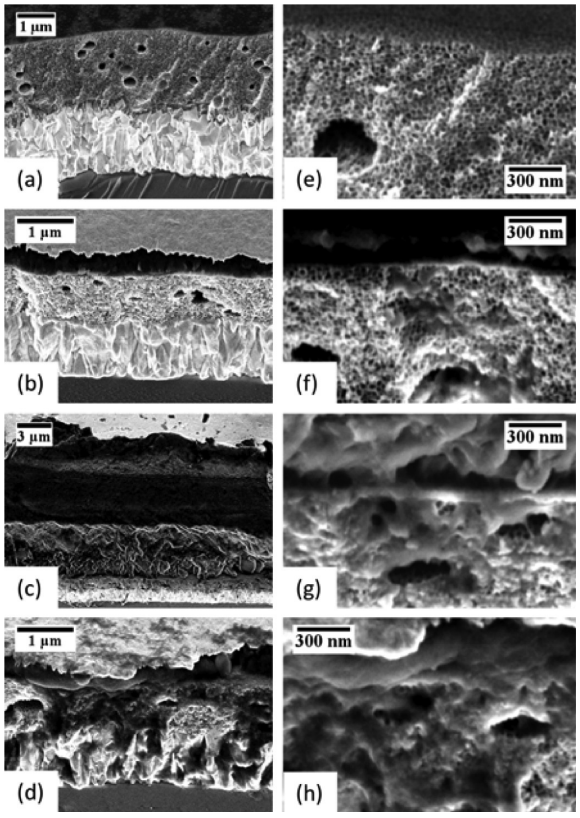

Figure 3. Cross-sectional SEM images of tailored titania sponge structure (a, e) and titania sponge structure filled with P3HT by 11 times repeated spin coating (b, f), filled with P3HT by solution casting (c, g), and filled with P3HT by soaking in toluene with subsequent spin coating (d, h). In the overview images (a–d), the FTO electrode on the bottom and the gold electrode on top of the P3HT (b–d) are visible.

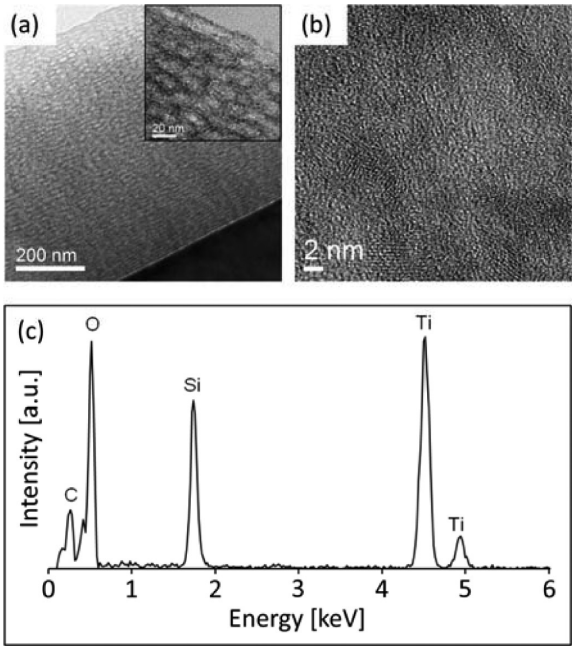

Figure 4. Bright field TEM image (a) of the tailored titania sponge structure. The inset shows the porous structure at higher magnification. The high-resolution TEM image in panel b displays one mesopore and several crystalline domains possessing diameters of 2–3 nm. In panel c, an exemplarily EDX spectrum taken in STEM mode is given of the 20 measured spectra used for the statistical analysis. In all 20 measured spectra, Si, Ti, O, and C are detected with a similar distribution.

spectra were taken at varying positions of the film. In Figure 4c, one exemplary EDX spectra is displayed. Si, Ti, C, and O are detected. The quantification of each EDX spectra reveals a similar distribution of Si and Ti and yields an average chemical composition of 43 ± 3 at.% Si and 57 ± 3 at.% Ti. As can be seen in the SEM images in Figure 3b–d and f–h, qualitatively, the pore-filling ratio increases from repeated spin coating of the hole-conductor via solution casting to soaking of the titania structures in toluene before spin coating of the hole-conductor solution for the defined titania sponge structures as well. Furthermore, the smaller pores seem to be filled more completely than the big pores. In addition, the titania film filled with P3HT by solution casting also shows a thick overlayer of P3HT, as visible in Figure 3c.

Reciprocal Space Morphology Analysis. To gain more quantitative information about the filling of the pores, the morphology is probed in reciprocal space with scattering techniques. TOF-GISANS measurements of the unfilled and filled structures have been performed. Figure 5 shows selected 2d scattering data of the granular titania structures, unfilled and, as an example, after filling with P3HT by soaking of the structures in toluene with subsequent spin coating of the polymer solution. The two-dimensional scattering shows very distinct features: at $q_y = q_z = 0$, the direct beam is probed, and the position in detector pixels drops for larger wavelengths due to the influence of gravity. For $q_y = 0$ and increasing values of q_z, above the direct beam, the minimum in intensity is due to the sample horizon above which the reflected signal is probed. The specularly reflected peak, for which incident and exit angles are equal, is probed always at the same pixel of the detector. Between sample horizon and specular peak, the Yoneda peak is detected.[76,77] As noted above, this maximum is moving with the wavelength of the neutron beam. For the short wavelengths in the TOF-GISANS experiment, the whole volume of the thin films is probed because the scattering depth is larger than 2 μm in case of the pure titania film and larger than 1 μm in case of the films filled with P3HT. For wavelengths in the TOF-GISANS experiment larger than 10 nm, only surface structures are probed at a scattering depth of minimum 60 nm in the case of the titania film and 40 nm in the case of the filled film. Scattering in the q_y direction is strongest for a q_z value of the Yoneda peak, where the scattering is most sensitive to the material under investigation. For the granular titania structures, a very broad scattering in the q_y direction is visible due to the broad distribution of lateral structure sizes in the probed films. To quantify this lateral size distribution, so-called horizontal cuts of the 2d TOF-GISANS data for the granular titania structure are shown in Figure 6. The cuts are fitted for all of the wavelengths by a model consisting of the form factor of two cylindrically shaped structures distributed on a 1d paracrystal; for the equations, see reference 79. For both the granular titania structure and the titania structure filled with P3HT by soaking in toluene with subsequent spin coating, lateral structure radii of (55 ± 15) and (10 ± 5) nm with distances of these structures of (180 ± 40) and (75 ± 20) nm are observed. Because of the very broad size distributions and as also no significant differences in the intensities in the horizontal cuts can be observed, the information about filling can not be extracted from the fits to the horizontal cuts. Furthermore, as

dx.doi.org/10.1021/am302255c | ACS Appl. Mater. Interfaces 2013, 5, 719–729

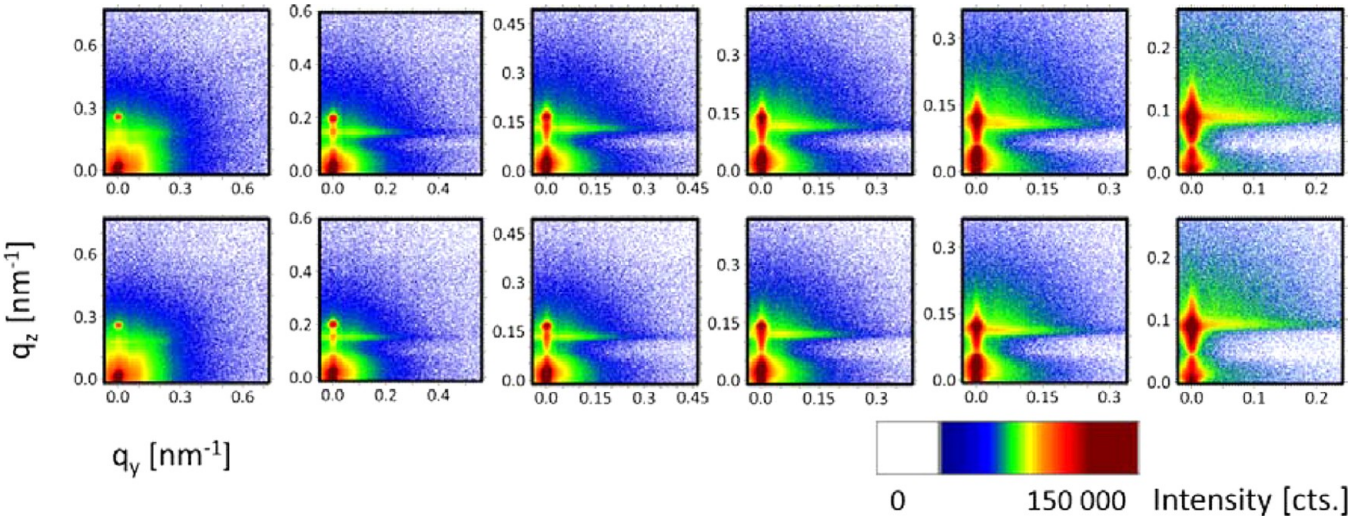

Figure 5. Selected 2d GISANS data: unfilled granular titania (top row) and granular titania filled with P3HT by soaking in toluene and subsequent spin coating (bottom row). The average wavelength of neutrons from left to right is 3.5, 4.5, 5.5, 6.5, 7.5, and 10.5 Å, respectively. The intensity scale (counts without normalization) is the same for all of the subfigures, the axis of abscissae shows q_y in inverse nm, and the axis of ordinates shows q_z in inverse nm. The different probed q ranges are due to the different wavelengths. Furthermore, the short wavelengths probe the structures in the whole volume of the films, and the longest shown wavelength probes only surface structures.

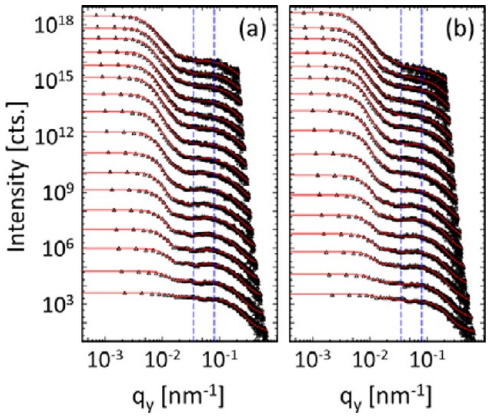

Figure 6. Horizontal cuts with fits of two broadly distributed cylindrically shaped objects, distributed on a 1d paracrystal as described in the text: Horizontal cuts are taken as an average of 15 pixels in q_z around the material characteristic scattering for the granular titania structure (a) and the granular titania structure filled with P3HT by soaking in toluene with subsequent spin coating (b). The cuts are taken around q_z values decreasing from 0.19 to 0.09 nm^{-1} for increasing wavelengths. The cuts of the 2d GISANS data for different wavelengths are shifted along the intensity axis with increasing wavelength from bottom to top without a normalization of the intensity. The different probed q ranges are due to the different wavelengths. The blue dashed lines indicate the distances of the two structures of around 180 and around 75 nm.

the probed structures do not differ much regardless of the wavelength of the neutrons, the surface structures do not differ from the structures in the volume of the film, in agreement with the observations in SEM.

The tailored titania sponge structures are also investigated with TOF-GISANS. Selected 2d scattering patterns are shown in Figure 7 for the pure titania structure and the titania structures filled in the investigated three different ways of P3HT infiltration. Already in the 2d scattering patterns, significant differences are visible. Concerning the scattering of the samples, the differences are apparent in the scattering in the q_y direction: First, the scattering is much more defined due to the presence of better defined structures in the samples. Second, the intensity of the scattering decreases from the unfilled titania structures with the expected more efficient filling from filling by repeated spin coating via filling by solution casting to filling by soaking in toluene with subsequent spin coating. This decrease in detected signal indicates strongly a more complete filling of the present pores as the scattering contrast is decreased for filled pores. Furthermore, again, the whole film volume is probed in the case of the measurements with the short neutron wavelengths (scattering depth of more than 2 μm and 1 μm, respectively, as explained above). For the longer wavelengths above 10 nm, surface structures are selectively probed, down to a minimum scattering depth of 70 nm in the case of the titania film and 35 nm in the case of the titania films filled with P3HT.

An additional difference in the 2d GISANS data arises from the usage of a beam stop that blocks the direct beam. However, the beam stop at the position of the directly transmitted beam is not affecting the reflected signal; therefore, the same information is available with or without beamstop.

To quantify the information of the lateral structures in the investigated samples, the horizontal line cuts, as depicted in Figure 8, are also fitted with a model consisting of the form factor of two cylindrically shaped structures distributed on a 1d paracrystal for all investigated wavelengths. Lateral structure radii of (38 ± 9) and (13 ± 6) nm with distances between these structures of (180 ± 40) and (25 ± 3) nm are observed. The structural distance of around 25 nm is well-defined, leading to the well-defined structural peak in the horizontal line cuts. As the well-defined peak is independent of the wavelength and consequently of the scattering depth, it can be concluded that the structure inside the film is independent of the depth in the film relative to the surface.[63,64] The probed distance can be related to the pore diameter of the titania sponge structure as observed with SEM in Figure 3a. The same observed structural features for the samples filled with P3HT show a decreasing intensity with expected increased filling: For the titania structure filled with P3HT by repeated spin coating, the

dx.doi.org/10.1021/am302255c | ACS Appl. Mater. Interfaces 2013, 5, 719−729

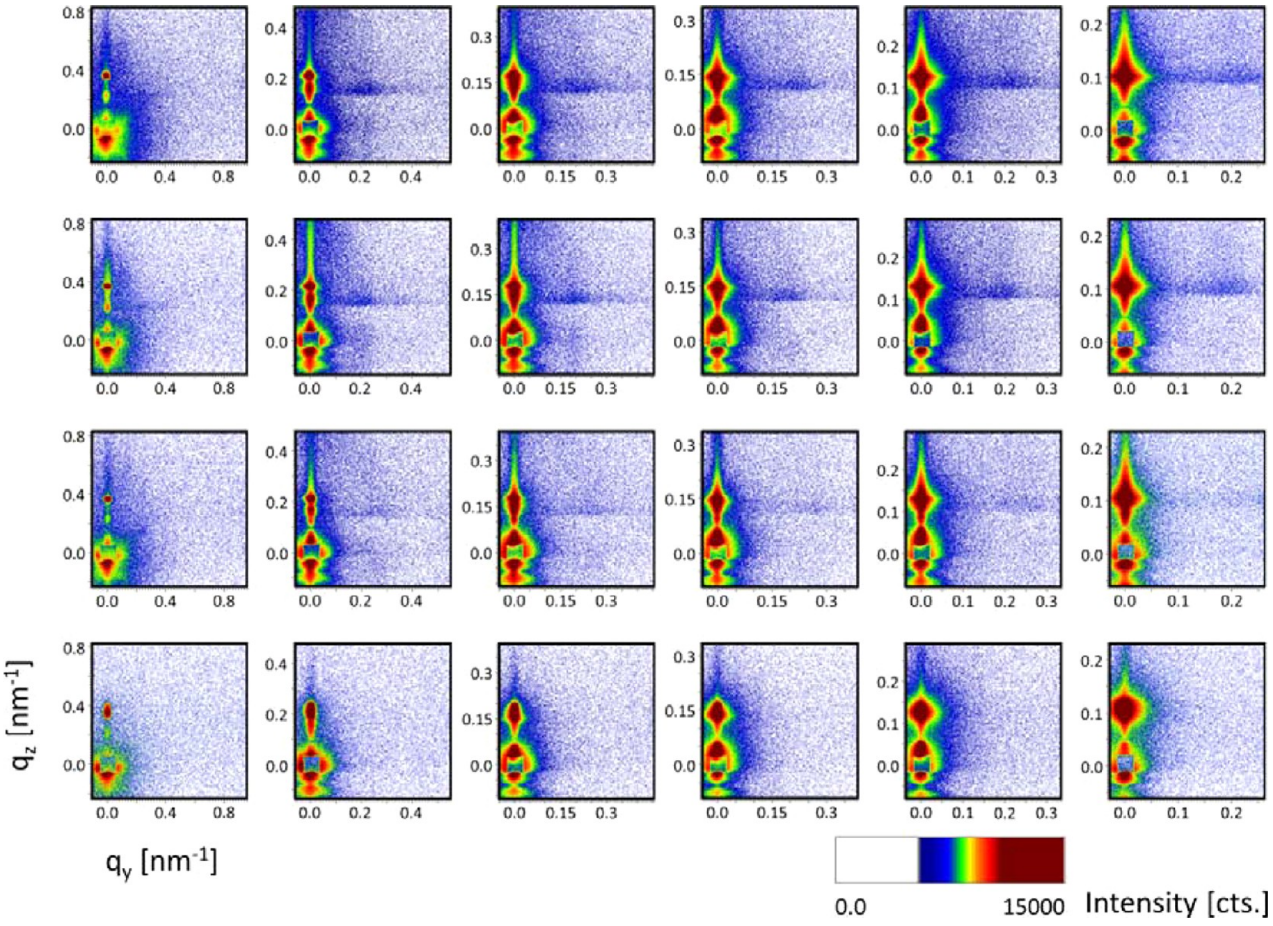

Figure 7. Selected 2d GISANS data: unfilled tailored titania sponge structure (top row) and tailored titania sponge structure filled by repeated 11 times spin coating (second row), filled by solution casting (third row), and filled by soaking in toluene with subsequent spin coating (bottom row). The average wavelength of neutrons from left to right is 2.6, 4.5, 5.5, 6.5, 7.5, and 9.5 Å, respectively. The intensity scale (counts without normalization) is the same for all of the subfigures, the axis of abscissae shows q_y in inverse nm, and the axis of ordinates shows q_z in inverse nm. The different probed q ranges are due to the different wavelengths. Furthermore, the short wavelengths probe the whole film volume, and in the case of the longest shown wavelength, only the surface structures are probed.

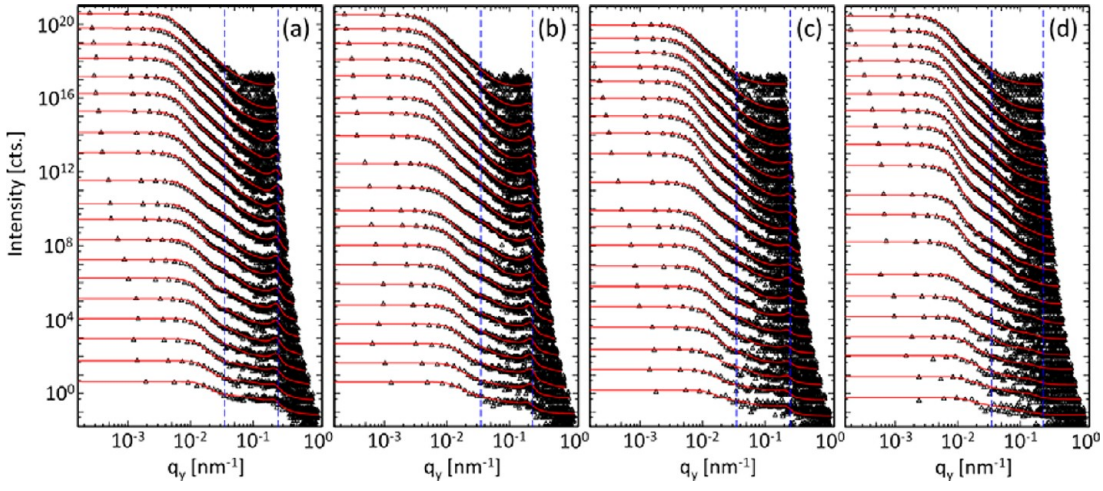

Figure 8. Horizontal cuts with fits of two cylindrically shaped geometries, distributed on a 1d paracrystal as described in the text: the cuts are taken as an average of 15 pixels in q_z around the characteristic scattering for the tailored titania sponge structure (a) and the titania sponge structure filled with P3HT by 11 times repeated spin coating (b), filled with P3HT by solution casting (c), and filled with P3HT by soaking in toluene with subsequent spin coating (d). From the shortest to the longest wavelengths, the cuts were performed around q_z values of 0.19 to 0.09 nm^{-1}. The cuts are shifted along the intensity axis with increasing wavelength from bottom to top without a normalization of the intensities, and the different probed q ranges are due to the different wavelengths. The blue dashed lines indicate the distances of the two probed structures of around 180 and around 25 nm.

dx.doi.org/10.1021/am302255c | ACS Appl. Mater. Interfaces 2013, 5, 719−729

scattering is reduced by a factor of about 65, and the distances are slightly increased to 27 nm. The slight increase in structure size might be due to partly filled small pores, which results in a slightly larger average pore distance. For the structure filled by solution casting, the scattering is reduced by a factor of about 290, and for filling by soaking in toluene with subsequent spin coating, the scattering is reduced by a factor of almost 20000.

Porosity and Degree of Filling. The porosity of the titania structures before filling and the degree of filling of the titania structures with P3HT is obtainable quantitatively from the vertical cuts of the TOF-GISANS data. By determining the critical angles from the Yoneda peaks for the different wavelengths used for the TOF-GISANS measurements and fitting of the critical angles versus wavelength, the SLD can be obtained from the slope of the linear fit as depicted in Figure 9

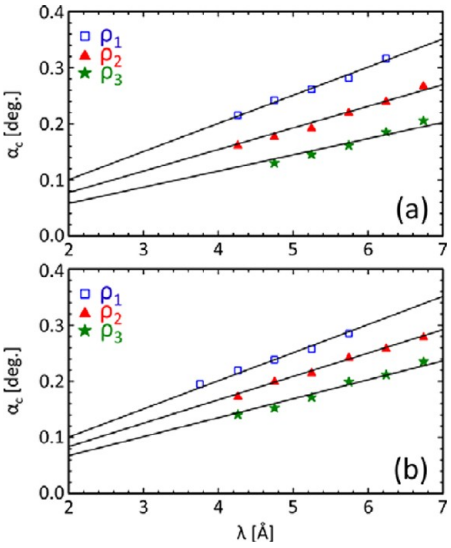

Figure 9. Linear fit of critical exit angles as obtained from TOF-GISANS data vs wavelength of neutrons for granular titania structure (a) and for unfilled granular titania filled with P3HT by soaking in toluene with subsequent spin coating (b). The fitted slopes are related to the density of compact titania (ρ_1) and the densities of the porous titania (ρ_2) and (ρ_3) in panel a and the titania partly filled with P3HT (ρ_2) and (ρ_3) in panel b, respectively, as described in the text.

for the data of the granular titania structures. For the analysis, only cuts of data are used that probe the whole film volume, as noted above. Therefore, the resulting values give the average of the whole film volume. In general, a rather broad distribution of Yoneda peaks is observed in the case of the unfilled granular titania structure, as can be seen in Figure 5. From the fits in Figure 9a, SLDs of $\rho_1 = 2.41 \times 10^{-6}$ Å^{-2}, $\rho_2 = 1.42 \times 10^{-6}$ Å^{-2}, and $\rho_3 = 8.0 \times 10^{-7}$ Å^{-2} are determined. The SLD ρ_1 corresponds to the SLD of a compact titania structure, and ρ_2 and ρ_3 are related to more porous titania layers with porosities of $\Phi_2 = 41\%$ and $\Phi_3 = 67\%$. Similarly, for the filled granular titania, SLDs of $\rho_1 = 2.41 \times 10^{-6}$ Å^{-2}, $\rho_2 = 1.67 \times 10^{-6}$ Å^{-2}, and $\rho_3 = 1.09 \times 10^{-6}$ Å^{-2} are determined. Again, the first SLD ρ_1 corresponds to the compact titania, and for the other two SLDs, the polymer fraction ξ inside the pores can be calculated. For the granular titania structures filled by P3HT via soaking in toluene with subsequent spin coating, filling ratios of $\xi_2 = 37\%$ and $\xi_3 = 44\%$ are determined. However, as a broad distribution of Yoneda peaks is observed, actually a broad distribution of porosities and a broad distribution of filling ratios in the observed range is expected to be present, where only the most prominent ones are determined.

Because of the absence of fringes in the intensity along q_z direction, no well-established depth profile exists inside the films in agreement with information extracted from different scattering depths.

For the unfilled tailored titania sponge structures, the porosity is more well-defined, as apparent from the more defined Yoneda peaks in the TOF-GISANS data in Figure 7. Also, the filled titania sponge structures show more defined Yoneda peaks, indicating more uniform filling with P3HT.

The critical angles as obtained from the Yoneda peaks are fitted linearly versus the wavelength of the neutrons, and the resulting plots are shown in Figure 10. Again, only data that probe the whole titania film volume are used; consequently, the determined values are averages over the whole film volume. For the unfilled titania sponge structure, SLDs of $\rho_1 = 3.52 \times 10^{-6}$

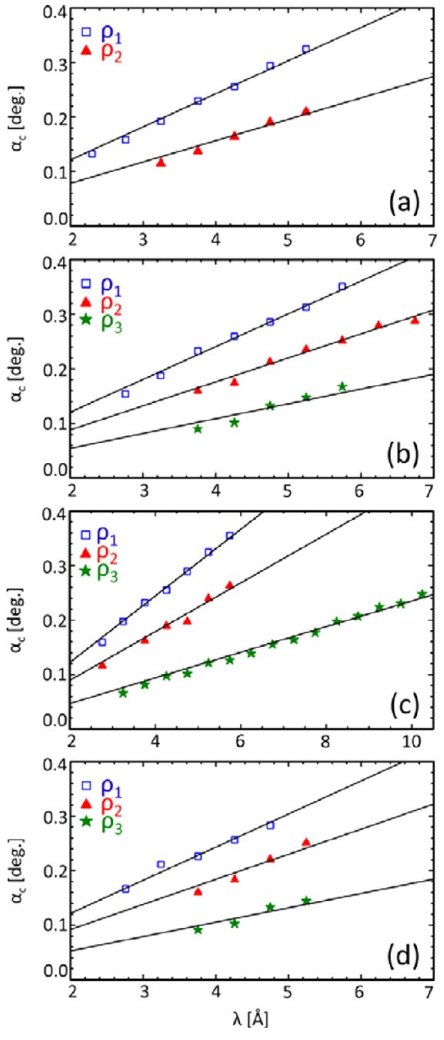

Figure 10. Linear fit of critical exit angles as obtained from the TOF-GISANS data vs wavelength of neutrons for the unfilled tailored titania sponge structure (a) and the titania sponge structure filled with P3HT by 11 times repeated spin coating (b), filled with P3HT by solution casting (c), and filled with P3HT by soaking in toluene with subsequent spin coating (d). The fitted slopes correspond to the density of the glass substrate (ρ_1), the density of the porous titania and the filled composite, respectively (ρ_2), and the pure P3HT overlayer (ρ_3).

dx.doi.org/10.1021/am302255c | ACS Appl. Mater. Interfaces 2013, 5, 719−729

$Å^{-2}$ and $\rho_2 = 1.47 \times 10^{-6}$ $Å^{-2}$ are determined from Figure 10a. The first SLD ρ_1 corresponds to the theoretical SLD of the glass substrate, which lies in the range of 3 to 4×10^{-6} $Å^{-2}$. The SLD of the substrate is visible for the titania sponge structures as the film thickness of these structures is lower than the film thickness of the granular titania, where the SLD of the silicon substrate was not visible in Figure 9. To determine the porosity of the titania sponge structure from the second SLD ρ_2, the theoretical SLD of the titania sponge structure is necessary as well. As the titania sponge structures actually consist of a mixture of titania and an SiOC type ceramic, an XRR measurement of the titania sponge is used in addition to determine the fraction of titania and SiOC. Figure 11 shows the

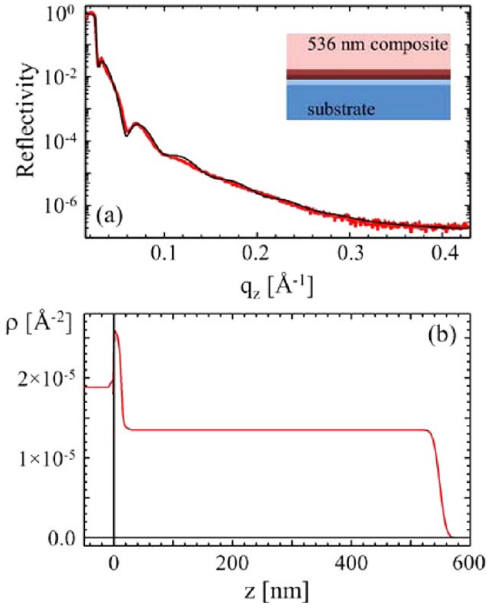

Figure 11. XRR curve (a) of the unfilled tailored titania sponge structure with fit (solid line) as described in the text. The SLD profile resulting from the fit (b) shown as a function of the distance z from the surface of the substrate at $z = 0$. The inset in panel a shows a sketch of the resulting vertical film composition: a 536 nm thick layer of the titania-ceramic composite with a porosity of 54% on top of more dense composite layers with in total 11 nm thickness resides on the glass substrate.

XRR data together with a fit to the data performed with the Parratt algorithm.[71] The vertical composition of the titania sponge structure is determined to be a 536 nm thick porous layer on top of in total 11 nm more dense titania layers near the glass substrate. The same depth profile of titania is not accessible by the GISANS data, as there are no intensity fringes present in the q_z cuts. In the fit to the XRR data, the film thickness is obtained from relative intensities at the edge of total external reflection. Fringes due to the layer thickness of around 536 nm are not resolved with XRR either. With the measured SLD for neutrons of $\rho_2 = 1.47 \times 10^{-6}$ $Å^{-2}$ and the SLD for X-rays obtained from the XRR fit as 1.35×10^{-5} $Å^{-2}$, the fraction of titania is obtained as 69%, and the fraction of SiOC is determined to be 31%. This titania fraction is higher but of similar order as the one obtained by EDX measurements.

The SLD of a compact material with this titania-ceramic composition for neutrons is 3.19×10^{-6} $Å^{-2}$. In total, the porosity Φ of the titania-ceramic composite sponge structure is determined to be 54%.

For the titania sponge structure filled with P3HT by 11 times repeated spin coating, the fit of critical angles versus wavelength as shown in Figure 10b results in SLDs of $\rho_1 = 3.56 \times 10^{-6}$ $Å^{-2}$, $\rho_2 = 1.76 \times 10^{-6}$ $Å^{-2}$, and $\rho_3 = 7.05 \times 10^{-7}$ $Å^{-2}$. The first SLD ρ_1 again corresponds to the SLD of the glass substrate. The third SLD ρ_3 is due to a compact P3HT layer. The intermediate SLD results from the titania-P3HT mixture, and a filling ratio of $\xi_2 = 57\%$ is determined for this way of filling.

In the case of filling of the titania sponge structure with P3HT by solution casting, the SLDs of $\rho_1 = 3.57 \times 10^{-6}$ $Å^{-2}$, $\rho_2 = 1.91 \times 10^{-6}$ $Å^{-2}$, and $\rho_3 = 5.28 \times 10^{-7}$ $Å^{-2}$ are determined from the fit of critical angle versus wavelength (Figure 10c). Again, ρ_1 is the SLD of the glass substrate, and ρ_3 is the SLD of a P3HT overlayer, which contains some 20% of air. As the Yoneda peak corresponding to the P3HT overlayer is scattering much more strongly than in the other cases, a much thicker overlayer of P3HT is present in the case of solution casting, as was already discussed to explain the bad solar cell efficiencies along with the SEM data. The intermediate SLD ρ_2 corresponds again to the titania-P3HT mixture, and a polymer fraction of $\xi_2 = 67\%$ is determined in the case of filling by solution casting.

Filling of the titania sponge structure by soaking in toluene with subsequent spin coating yields SLD values of $\rho_1 = 3.53 \times 10^{-6}$ $Å^{-2}$, $\rho_2 = 2.03 \times 10^{-6}$ $Å^{-2}$, and $\rho_3 = 6.64 \times 10^{-7}$ $Å^{-2}$ as determined from the fit of critical angles versus wavelength in Figure 10d. In accordance with the other filled samples, ρ_1 is the SLD of the glass substrate, and ρ_3 is the SLD of a P3HT overlayer. A polymer fraction of $\xi_2 = 84\%$ is determined from the intermediate SLD ρ_2 in the case of filling by soaking in toluene with subsequent spin coating. An overview of all determined porosity values and degrees of filling is given in Table 2.

Table 2. Overview of Porosity and Degree of Filling Values for the Different Kinds of P3HT Infiltration into the Granular Titania and the Tailored Titania Nanostructure

	porosity	degree of filling
granular titania	41 and 67%	–
granular titania filled by spin coating after soaking in toluene	–	37 and 44%
tailored titania	54%	–
tailored titania filled by 11 times spin coating	–	57%
tailored titania filled by solution casting	–	67%
tailored titania filled by spin coating after soaking in toluene	–	84%

In comparison to the literature, where quantitatively just 25% filling in the case of one time spin coating and 67% filling in the case of solution casting was observed for a similar titania structure but a different conducting polymer,[62] in the present investigation, a filling of 57% for 11 times repeated spin coating is observed, which is higher than the filling ratio for one time spin coating, as expected. Sixty-seven percent filling for solution casting is observed in the present investigation as well. Thus, the degree of filling seems to be rather independent of the used polymer for a similar titania structure for this type of technique. The filling ratio of 84% for the infiltration by soaking in toluene with subsequent spin coating is clearly larger than for the other ways of polymer infiltration, in agreement with the local probe SEM and explaining well the better solar cell performance for

dx.doi.org/10.1021/am302255c | ACS Appl. Mater. Interfaces 2013, 5, 719–729

solar cells prepared by filling of the tiania structure with the hole-conductor P3HT by this method.

CONCLUSIONS

The filling of different titania structures with the hole-conductor P3HT is compared for three ways of infiltration. Even though no record solar cells are investigated, principle findings in the comparison of titania films obtained from a commercial paste with films containing tailored sponge titania nanostructures via block copolymer templating allow for the optimization of future applications on the basis of quantitative results. In ssDSSCs, infiltration of the P3HT by solution casting shows the worst performance, whereas both infiltration by 11 times repeated spin coating and infiltration by soaking in the solvent with subsequent spin coating lead to reasonable results, with a higher short-cut current for the infiltration by soaking in the solvent with subsequent spin coating.

For both granular titania structures as they are applied commercially and tailored titania sponge structures, an increasing filling of the pores in the titania structures with P3HT is observed from filling by repeated spin coating via filling by solution casting to filling by soaking in the solvent with subsequent spin coating. For the sponge structure, the porosity of the original structure is 54%, and regular well-defined porous structures are observed. The filling ratios of the pores can be determined with a good statistical relevance to 57, 67, and 84% for the three different ways of filling from TOF-GISANS measurements. For the granular titania structures, a large distribution of pores and porosity values in the range of 41−67% is present before filling with P3HT. For the filling by soaking in the solvent with subsequent spin coating, filling ratios of 37−44% are obtained. In addition, a rather thick overlayer of P3HT is observed in the case of solution casting for both titania structures, which leads to the bad solar cell performance for this way of filling. As the goal of the present studies is not to optimize one way of filling, but the comparison of all advantages and disadvantages, the overlayer was not removed. The removal of the overlayer would again promise increased solar cell efficiencies, with the disadvantage of a further preparation step. For the filling by repeated spin coating or spin coating subsequent to soaking in the solvent, a similarly thin overlayer is observed, leading to improved solar cell efficiencies by improved filling alone.

In conclusion, the degree of filling depends strongly on the morphology of the titania structure that is to be filled: More regular structures are easier to fill than structures with broad distributions of sizes. For similar structures, the filling does not depend much on the hole-conducting polymer used for the filling. A better filling in otherwise identical ssDSSCs leads to a better solar cell performance. The filling by soaking of the structures in the solvent with subsequent spin coating is proposed for high filling ratios of well-ordered titania structures.

AUTHOR INFORMATION

Corresponding Author

*Tel: +49 (0)89 289 12451. Fax: +49 (0)89 289 12473. E-mail: muellerb@ph.tum.de.

Present Address

§Deutsches Textilforschungszentrum Nord-West e.V., Institut an der Universität Duisburg-Essen, Adlerstrasse 1, 47798 Krefeld, Germany.

Author Contributions

All authors have given approval to the final version of the manuscript.

Notes

The authors declare no competing financial interest.

ACKNOWLEDGMENTS

We are grateful to P. Weiser and A. Holleitner for the possibility to perform SEM measurements and to D. Magerl for the implementation of the horizontal line cut fit model. Moreover, we thank A. Kriele and P. Link for the support during the XRR measurements. The financial support of the Deutsche Forschungsgemeinschaft in the priority program SPP 1181 "Nanomat" (MU1487/5 and GU771/2) and in the frame of in the Bavarian Collaborative Research Project "Solar technologies go Hybrid" (SolTec) via TUM.solar is gratefully acknowledged. C.S. and A.W. acknowledge financial support from the cluster of excellence Nanosystems Initiative Munich (NIM).

REFERENCES

(1) O'Regan, B.; Grätzel, M. *Nature* **1991**, *353*, 737−740.
(2) Grätzel, M. *J. Photochem. Photobiol., C* **2003**, *4*, 145−153.
(3) Hardin, B. E.; Snaith, H. J.; McGehee, M. D. *Nat. Photonics* **2012**, *6*, 162−169.
(4) International Energy Agency (IEA). *Technology Roadmap—Solar Photovoltaic Energy*, 2010.
(5) Hagen, J.; Schaffrath, W.; Otschik, P.; Fink, R.; Bacher, A.; Schmidt, H.-W.; Haarer, D. *Synth. Met.* **1997**, *89*, 215−220.
(6) Schmidt-Mende, L.; Grätzel, M. *Thin Solid Films* **2006**, *500*, 296−301.
(7) Snaith, H. J.; Humphry-Baker, R.; Chen, P.; Cesar, I.; Zakeeruddin, S. M.; Grätzel, M. *Nanotechnology* **2008**, *19*, 424003.
(8) Snaith, H. J.; Schmidt-Mende, L. *Adv. Mater.* **2007**, *19*, 3187−3200.
(9) Kroeze, J. E.; Hirata, N.; Schmidt-Mende, L.; Orizu, C.; Ogier, S. D.; Carr, K.; Grätzel, M.; Durrant, J. R. *Adv. Funct. Mater.* **2006**, *16*, 1832−1838.
(10) Bartholomew, G. P.; Heeger, A. J. *Adv. Funct. Mater.* **2005**, *15*, 677−682.
(11) Coakley, K. M.; Liu, Y.; McGehee, M. D.; Frindell, K. L.; Stucky, G. D. *Adv. Funct. Mater.* **2003**, *13*, 301−306.
(12) Coakley, K. M.; McGehee, M. D. *Appl. Phys. Lett.* **2003**, *83*, 3380−3382.
(13) Coakley, K. M.; Srinivasan, B. S.; Ziebarth, J. M.; Goh, C.; Liu, Y.; McGehee, M. D. *Adv. Funct. Mater.* **2005**, *15*, 1927−1932.
(14) De Sio, A.; Madena, T.; Huber, R.; Parisi, J.; Neyshtadt, S.; Deschler, F.; Da Combo, E.; Esposito, S.; von Hauff, E. *Sol. Energy Sol. Cells* **2011**, *95*, 3536−3542.
(15) Chen, X.; Mao, S. S. *Chem. Rev.* **2007**, *107*, 2891−2959.
(16) Barbé, C. J.; Arendse, F.; Comte, P.; Jirousek, M.; Lenzmann, F.; Shklover, V.; Grätzel, M. *J. Am. Ceram. Soc.* **1997**, *80*, 3157−3171.
(17) Ahmed, S.; Du Pasquier, A.; Birnie, D. P.; Asefa, T. *ACS Appl. Mater. Interfaces* **2011**, *3*, 3002−3010.
(18) Lee, K. S.; Kwon, J.; Im, J. H.; Lee, C. R.; Park, N.-G.; Park, J.-H. *ACS Appl. Mater. Interfaces* **2012**, *4*, 4164−4168.
(19) Ghosh, R.; Brennaman, M. K.; Uher, T.; Ok, M.-R.; Samulski, E. T.; McNeil, L. E.; Meyer, T. J.; Lopez, R. *ACS Appl. Mater. Interfaces* **2011**, *3*, 3929−3935.
(20) Ameen, S.; Akhtar, M. S.; Song, M.; Shin, H. S. *ACS Appl. Mater. Interfaces* **2012**, *4*, 4405−4412.
(21) Williams, V. O.; Jeong, N. C.; Prasittichai, C.; Farha, O. K.; Pellin, M., J.; Hupp, J. T. *ACS Nano* **2012**, *6*, 6185−6196.
(22) Sessolo, M.; Bolink, H. J. *Adv. Mater.* **2011**, *23*, 1829−1845.
(23) Sanchez, C.; Boissière, C.; Grosso, D.; Laberty, C.; Nicole, L. *Chem. Mater.* **2008**, *20*, 682−737.

(24) Kettunen, M.; Silvenoinen, R. J.; Houbenov, N.; Nykänen, A.; Ruokolainen, J.; Sainio, J.; Pore, V.; Kemell, M.; Ankerfors, M.; Lindström, T.; Ritala, M.; Ras, R. H. A.; Ikkala, O. *Adv. Funct. Mater.* **2011**, *21*, 510−517.
(25) Wessel, C.; Ostermann, R.; Dersch, R.; Smarsly, B. M. *J. Phys. Chem. C* **2011**, *115*, 362−372.
(26) Kim, M. H.; Baik, J. M.; Zhang, J.; Larson, C.; Li, Y.; Stucky, G. D.; Moskovits, M.; Wodtke, A. M. *J. Phys. Chem. C* **2010**, *114*, 10697−10702.
(27) Mor, G. K.; Varghese, O. K.; Paulose, M.; Shankar, K.; Grimes, C. A. *Sol. Energy Mater. Sol. Cells* **2006**, *90*, 2011−2075.
(28) Roy, P.; Berger, S.; Schmuki, P. *Angew. Chem., Int. Ed.* **2011**, *50*, 2904−2939.
(29) Weickert, J.; Palumbiny, C.; Nedelcu, M.; Bein, T.; Schmidt-Mende, L. *Chem. Mater.* **2011**, *23*, 155−162.
(30) Caruso, F.; Shi, X.; Caruso, R. A.; Susha, A. *Adv. Mater.* **2001**, *13*, 740−744.
(31) Cölfen, H.; Antonietti, M. *Angew. Chem., Int. Ed.* **2005**, *44*, 5576−5591.
(32) Crepaldi, E. L.; Soler-Illia, G. J. de A. A.; Grosso, D.; Cagnol, F.; Ribot, F.; Sanchez, C. *J. Am. Chem. Soc.* **2003**, *125*, 9770−9786.
(33) Orilall, M. C.; Wiesner, U. *Chem. Soc. Rev.* **2011**, *40*, 520−535.
(34) Rawolle, M.; Braden, E. V.; Niedermeier, M. A.; Magerl, D.; Sarkar, K.; Fröschl, T.; Hüsing, N.; Perlich, J.; Müller-Buschbaum, P. *ChemPhysChem* **2012**, *13*, 2412−2417.
(35) Rauda, I. E.; Buonsanti, R.; Saldarriaga-Lopez, L. C.; Benjauthrit, K.; Schelhas, L. T.; Stefik, M.; Augustyn, V.; Ko, J.; Wiesner, U.; Milliron, D. J.; Tolbert, S. H. *ACS Nano* **2012**, *6*, 6386−6399.
(36) Rawolle, M.; Niedermeier, M. A.; Kaune, G.; Perlich, J.; Lellig, P.; Memesa, M.; Cheng, Y.-J.; Gutmann, J. S.; Müller-Buschbaum, P. *Chem. Soc. Rev.* **2012**, *41*, 5131−5142.
(37) Stefik, M.; Lee, J.; Wiesner, U. *Chem. Commun.* **2009**, 2532−2534.
(38) Cheng, Y.-J.; Gutmann, J. S. *J. Am. Chem. Soc.* **2006**, *128*, 4658−4674.
(39) Yu, K.; Eisenberg, A. *Macromolecules* **1996**, *29*, 6359−6361.
(40) Zhang, Y.; Tan, H.; Li, H.; Liu, Y.-Q.; Kartawidjaja, F. C.; Yang, Z.-C.; Wang, J. *Chem. Mater.* **2011**, *23*, 2745−2752.
(41) Niedermeier, M. A.; Magerl, D.; Zhong, Q.; Nathan, A.; Körstgens, V.; Perlich, J.; Roth, S. V.; Müller-Buschbaum, P. *Nanotechnology* **2012**, *23*, 145602.
(42) Fuertes, M. C.; Soler-Illia, G. J. A. A. *Chem. Mater.* **2006**, *18*, 2109−2117.
(43) Koganti, V. R.; Dunphy, D.; Gowrishankar, V.; McGehee, M. D.; Li, X.; Wang, J.; Rankin, S. E. *Nano Lett.* **2006**, *6*, 2567−2570.
(44) Nedelcu, M.; Lee, J.; Crossland, E. J. W.; Warren, S. C.; Orilall, M. C.; Guldin, S.; Hüttner, S.; Ducati, C.; Eder, D.; Wiesner, U.; Steiner, U.; Snaith, H. J. *Soft Matter* **2009**, *5*, 134−139.
(45) Andreasen, J. W.; Jorgensen, M.; Krebs, F., C. *Macromolecules* **2007**, *40*, 7758−7762.
(46) Ruderer, M. A.; Müller-Buschbaum, P. *Soft Matter* **2011**, *7*, 5482−5493.
(47) Förster, S.; Timmann, A.; Konrad, M.; Schellbach, C.; Meyer, A.; Funari, S. S.; Mulvaney, P.; Knott, R. *J. Phys. Chem. B* **2005**, *109*, 1347−1360.
(48) Kaune, G.; Ruderer, M. A.; Metwalli, E.; Wang, W.; Couet, S.; Schlage, K.; Röhlsberger, R.; Roth, S. V.; Müller-Buschbaum, P. *ACS Appl. Mater. Interfaces* **2009**, *1*, 353−360.
(49) Fischereder, A.; Rath, T.; Haas, W.; Amenitsch, H.; Schenk, D.; Zankel, A.; Saf, R.; Hofer, F.; Trimmel, G. *ACS Appl. Mater. Interfaces* **2012**, *4*, 382−390.
(50) Salditt, T.; Brotons, G. *Anal. Bioanal. Chem.* **2004**, *379*, 960−973.
(51) Wolff, M.; Magerl, A.; Zabel, H. *Eur. Phys. J. E* **2005**, *16*, 141−145.
(52) Penfold, J.; Ward, R. C.; Williams, W. G. *J. Phys. E.: Sci. Instrum.* **1987**, *20*, 1411−1417.
(53) Karim, A.; Arendt, B. H.; Goyette, R.; Huang, Y. Y.; Kleb, R.; Felcher, G. P. *Phys. B* **1991**, *173*, 17−24.
(54) Bucknall, D. G.; Butler, S. A.; Higgins, J. S. *J. Phys. Chem. Solids* **1999**, *60*, 1273−1277.
(55) Gutberlet, T.; Steitz, R.; Fragneto, G.; Klösgen, B. *J. Phys.: Condens. Matter* **2004**, *16*, S2469−S2476.
(56) Felcher, G. P.; te Velthuis, S. G. E. *Appl. Surf. Sci.* **2001**, *182*, 209−215.
(57) Lee, W.-T.; Klose, F.; Yin, H. Q.; Toperverg, B. P. *Phys. B* **2003**, *335*, 77−81.
(58) Ott, F.; Menelle, A.; Fermon, C.; Humbert, P. *Phys. B* **2000**, *283*, 418−421.
(59) Salditt, T.; Münster, C.; Mennicke, U.; Ollinger, C.; Fragneto, G. *Langmuir* **2003**, *19*, 7703−7711.
(60) Müller-Buschbaum, P.; Metwalli, E.; Moulin, J.-F.; Kudryashov, V.; Haese-Seiller, M.; Kampmann, R. *Eur. Phys. J. Spec. Top.* **2009**, *167*, 107−112.
(61) Kreuzpaintner, W.; Moulin, J.-F.; Lott, D.; Kampmann, R.; Haese-Seiller, M.; Störmer, M.; Schreyer, A. *Eur. Phys. J. Spec. Top.* **2009**, *167*, 73−79.
(62) Kaune, G.; Haese-Seiller, M.; Kampmann, R.; Moulin, J.-F.; Zhong, Q.; Müller-Buschbaum, P. *J. Polym. Sci. B: Polym. Phys.* **2010**, *48*, 1628−1635.
(63) Müller-Buschbaum, P.; Schulz, L.; Metwalli, E.; Moulin, J.-F.; Cubitt, R. *Langmuir* **2008**, *24*, 7639−7644.
(64) Kerscher, M.; Busch, P.; Mattauch, S.; Frielinghaus, H.; Richter, D.; Belushkin, M.; Gompper, G. *Phys. Rev. E* **2011**, *83*, 030401(R).
(65) Lellig, P.; Niedermeier, M. A.; Rawolle, M.; Meister, M.; Laquai, F.; Müller-Buschbaum, P.; Gutmann, J. S. *Phys. Chem. Chem. Phys.* **2012**, *14*, 1607−1613.
(66) Yu, H.; Zhang, S.; Zhao, H.; Will, G.; Liu, P. *Electrochim. Acta* **2009**, *54*, 1319−1324.
(67) Müller-Buschbaum, P. *Eur. Phys. J. E* **2003**, *12*, 443−448.
(68) Rawolle, M.; Ruderer, M. A.; Prams, S. M.; Zhong, Q.; Magerl, D.; Perlich, J.; Roth, S. V.; Lellig, P.; Gutmann, J. S.; Müller-Buschbaum, P. *Small* **2011**, *7*, 884−891.
(69) Kaune, G.; Memesa, M.; Meier, R.; Ruderer, M. A.; Diethert, A.; Roth, S. V.; D'Acunzi, M.; Gutmann, J. S.; Müller-Buschbaum, P. *ACS Appl. Mater. Interfaces* **2009**, *1*, 2862−2869.
(70) Lal, J.; Gilbert, E. P.; Auvray, L. *Phys. A* **2002**, *304*, 244−248.
(71) Parratt, L. G. *Phys. Rev.* **1954**, *95*, 359−369.
(72) Strecker, A.; Salzberger, U.; Mayer, J. *Prakt. Metallogr.* **1993**, *30*, 482.
(73) Kampmann, R.; Haese-Seiller, M.; Kudryashov, V.; Deriglazov, V.; Tristl, M.; Daniel, Ch.; Toperverg, B.; Schreyer, A.; Sackmann, E. *Phys. B* **2004**, *350*, e763−e766.
(74) Kampmann, R.; Haese-Seiller, M.; Kudryashov, V.; Nickel, B.; Daniel, C.; Fenzl, W.; Schreyer, A.; Sackmann, E.; Rädler, J. *Phys. B* **2006**, *385−386*, 1161−1163.
(75) Kampann, R.; Marmotti, M.; Haese-Seiller, M.; Kudryashov, V. *Nucl. Instrum. Methods A* **2004**, *529*, 342−347.
(76) Yoneda, Y. *Phys. Rev.* **1963**, *131*, 2010−2013.
(77) Sinha, S. K.; Sirota, E. B.; Garoff, S.; Stanley, H. B. *Phys. Rev. B* **1988**, *38*, 2297−2312.
(78) Dosch, H.; Batterman, B. W.; Wack, D. C. *Phys. Rev. Lett.* **1986**, *56*, 1144−1147.
(79) Lazzari, R. *J. Appl. Crystallogr.* **2002**, *35*, 406−421.